Measuring Directionality in Double Beta Decay and Neutrino Interactions with Kiloton-Scale Scintillation Detectors

C. Aberle,[1] A. Elagin,[2] M. Wetstein,[2] H. J. Frisch,[2] and L. Winslow[1]

[1]*University of California Los Angeles, Los Angeles, CA 90095, USA*
[2]*University of Chicago, Chicago, IL, 60637, USA*

(Dated: July 19, 2013)

Large liquid-scintillator-based detectors have proven to be exceptionally effective for low energy neutrino measurements due to their good energy resolution and scalability to large volumes. The addition of directional information using Cherenkov light and fast timing would greatly enhance the scientific reach of these detectors, especially for searches for neutrinoless double-beta decay. In this paper, we develop a technique for extracting particle direction and evaluate different detector advances that could be used to make direction reconstruction a reality in a kiloton-scale detector.

PACS numbers: 23.40.−s, 21.10.Tg, 14.60.Pq, 27.60.+j

I. INTRODUCTION

Liquid scintillator based detectors are responsible for several of the critical measurements that have determined our present understanding of neutrino masses and mixings. These measurements include KamLAND's measurement of reactor antineutrino oscillation at a distance of $\sim$200 km[1], Borexino's measurement of ^{7}Be solar neutrino oscillation[2], and most recently the short baseline reactor antineutrino experiments that measured oscillations due to θ_{13} at a distance of 1 km: Daya Bay[3], Double Chooz[4, 5], and RENO[6]. Scintillator-based neutrino detectors will continue to be important for the next set of neutrino measurements, from the determination of the neutrino mass hierarchy[7, 8] to elastic scattering measurements[9] and sterile neutrino searches[10, 11] and for non-proliferation applications[12, 13].

The scalability of these detectors to large volumes also makes them highly competitive for neutrinoless double-beta ($0\nu\beta\beta$) decay searches in which the final state consists of a positron-electron pair with energies in the few MeV range. Currently one of the best limits for the $0\nu\beta\beta$ half-life comes from KamLAND-Zen[14].

The advantage of liquid scintillators for measurements in the $\sim$1 MeV range is their scalability from 1 ton to 1 kiloton while providing energy resolutions of $\sim$5%. This is roughly a factor of two better than water Cerenkov detectors, the other developed technology that can be economically scaled to these large masses. However, for scintillator-based detectors, while the energy resolution is good due to the abundance of light, the light is isotropic and does not retain the directional information of the primary particle. In contrast, the direction of the particle can be reconstructed from the Cerenkov cones in water-based detectors, although the energy resolution rapidly degrades below $\sim$5 MeV. For double-beta decay in particular, but also for neutrino interactions, the directional information can be a strong suppressant of backgrounds.

In a liquid-scintillation-based detector, Cerenkov light is also produced, although most is absorbed and re-emitted as part of the scintillation processes. However, some fraction retains its directional information. If this directional Cerenkov light can be isolated from the copious isotropic scintillation light, it may be possible to reconstruct the direction of the primary particle or, in the case of double beta decay, to determine the existence and topology of the pair. The addition of directionality is thus a powerful tool for background rejection. In this paper, we develop a technique for separating the Cerenkov and scintillation using the photon arrival times and evaluate different detector technologies that would allow the realization direction reconstruction in kilo-ton scale scintillating neutrino detectors.

II. LIGHT PRODUCTION IN LIQUID SCINTILLATORS

Liquid scintillators are cocktails of aromatic hydrocarbons. When charged particles move through a scintillator, the molecules are excited, predominantly the the non-localized electrons in the π-bonds of the phenyl groups [15]. Vibrational and rotational modes of the molecules are turned into heat within picoseconds through collisions with other molecules. Within $\sim$10 picoseconds, the π-electrons de-excite to the first excited state from higher levels through radiationless transitions. The first excited state de-excites through photon emission. There are two characteristic times for this de-excitation, depending if the singlet state or the triplet state was excited. The singlet state will de-excite within nanoseconds while the triplet state de-excites on the order of 10's or 100's of nanoseconds. These two processes are fluorescence and phosphorescence respectively. The exact time constants for these processes are determined by the composition of the scintillator.

The molecules in liquid scintillators are not isolated. Radiationless processes transfer energy between the molecules. The probability of energy transfer between molecules increases as the overlap between the molecule's absorption and emission spectra increase. The absorption and emission spectra overlap at some level for all molecules. Consequently if there is only one type of molecule in the scintillator cocktail, the light output would be reduced due to inefficiencies in the energy transfer through multiple absorption and reemission processes. Aromatic solutes or fluors are added to the primary solvent to shift the wavelength of the photons to longer

wavelengths where the scintillator is more transparent. This wavelength-shifting is also used to match the quantum efficiency as a function of wavelength for the photodetectors being used. One typical scintillator mixture uses pseudo-cumene as the solvent with 1-5 g/L of PPO as the fluor. This mixture has a peak emission at about 400 nm where bialkali photomultiplier tubes (PMTs) are most sensitive and the pseudocumene is relatively transparent.

A good liquid scintillator will produce ∼10,000 photons isotropically per MeV of deposited energy. Although less abundant, Cerenkov light will be produced as well if a particle is moving faster than the speed of light in the medium. This light is emitted in a cone pointed in the direction of the particles trajectory and with a continuous spectrum weighted toward shorter wavelengths but extending well into the red. The spectrum is described by:

$$\frac{dN}{d\lambda dx} = \frac{2\pi\alpha Z^2}{\lambda^2}(1 - \frac{1}{\beta^2 n(\lambda)^2}) \quad (1)$$

where $n(\lambda)$ is the wavelength-dependent index of refraction and β is the velocity of the incoming particle. The Cerenkov light produced at wavelengths shorter than the absorption cutoff of the scintillator will be absorbed and re-emitted as isotropic light, but wavelengths longer than this cutoff will propagate across the detector, retaining their directional information. The yield is roughly 60 photons per MeV, assuming a 400 nm absorption cutoff[16]. These undisturbed Cerenkov photons will have timing determined by the group velocity [17] in the liquid,

$$v_g(\lambda) = \frac{c_{vacuum}}{n(\lambda) - dn(\lambda)/d\log(\lambda)}. \quad (2)$$

In Geant4 optical photons are assigned the group velocity in the wavelength region of normal dispersion which is relevant to our study. The longer wavelengths Cerenkov photons typically arrive before the scintillation light, which is slowed by both the scintillation processes and the shorter wavelengths involved. Thus, with sufficient timing resolution and sensitivity to longer wavelength, it should be possible to separate the directional Cerenkov light and the isotropic scintillation light in time and then reconstruct the direction of the initial particle.

III. GEANT4 SIMULATION

In order to study the effects relevant to directionality reconstruction in liquid scintillators, a Geant4 [18, 19] simulation has been set up. The presented simulation has been developed using standard Geant4 (version 4.9.6) functionality for the liquid scintillator optical model. The simulation has been built from a customized official Geant4 application example and it is kept rather generic to provide generally applicable information about the main factors in directionality reconstruction.

The implemented detector geometry is a sphere of 6.5 m diameter filled with liquid scintillator (see Figure 1). Default scintillator properties have been chosen to match the

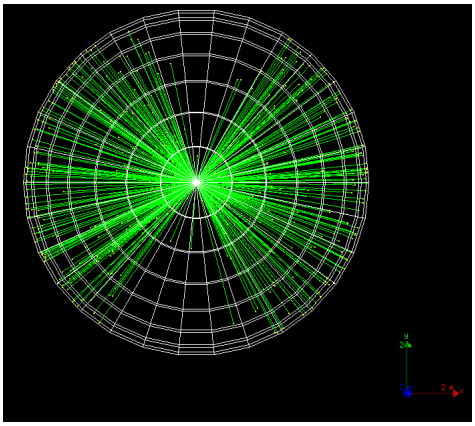

FIG. 1: Two back-to-back electrons with 1.41 MeV each (equally divided energy of ^{1}16Cd $0\nu\beta\beta$ decay) at the center of the sphere with initial directions along the x and -x-axis. Only Cerenkov photons are drawn to illustrate the directionality of the event.

KamLAND scintillator [20]: 80 % n-Dodecane, 20 % Pseudocumene (1,2,4-Trimethylbenzene) and 1.52 g/l PPO (2,5-Diphenyloxazole). The implemented scintillator properties include the atomic composition and density (ρ = 0.78 g/ml), the wavelength-dependent attenuation length [21] and refractive index [22], the scintillation emission spectrum, emission rise time (τ_r = 1.0 ns) and emission decay time constants (τ_{d1} = 6.9 ns and τ_{d2} = 8.8 ns with relative weights of 0.87 and 0.13) [23], scintillator light yield (LY, 9030 photons/MeV) and the Birks constant ($kB \approx 0.1$ mm/MeV) [24]. Variations from the baseline KamLAND case are discussed below when applicable. Reflections, reemission of absorbed photons in the scintillator bulk volume and scattering has not been included. These effects are expected to be corrections to the main effects studied in this paper and are subject of future work.

The inner sphere surface is used as the photodetector. It is treated as fully absorbing (no reflections) with a photodetector coverage of 100 %. Two important photodetector properties have been varied: Transit time spread (TTS, default σ = 0.1 ns) and wavelength-dependent quantum efficiency (QE) for photoelectron production. Default is the QE of a bialkali photocathode (Hamamatsu R7081 PMT), digitized values come from the Double Chooz [4] Monte Carlo simulation. We note that the KamLAND 17 inch PMTs use the same photocathode type (bialkali) with similar quantum efficiency.

Before the simulation results for different simulation settings are discussed in the following sections, we highlight the effects which contribute to the timing of the scintillator detector system. First, the simulated travel time of the initial 5 MeV electron is between 0.10 and 0.15 ns, while the travel distance is about 3 cm. Second, the scintillation light emission follows a scintillator-specific distribution characterized by rise and decay time(s). Before the solutes in liquid scintillator can emit optical photons, the energy has to be transfered from the solvent to the solute. The time constant of this energy transfer accounts for a rise time in scintillation light emission. Past neutrino experiments were not highly interested in the effect

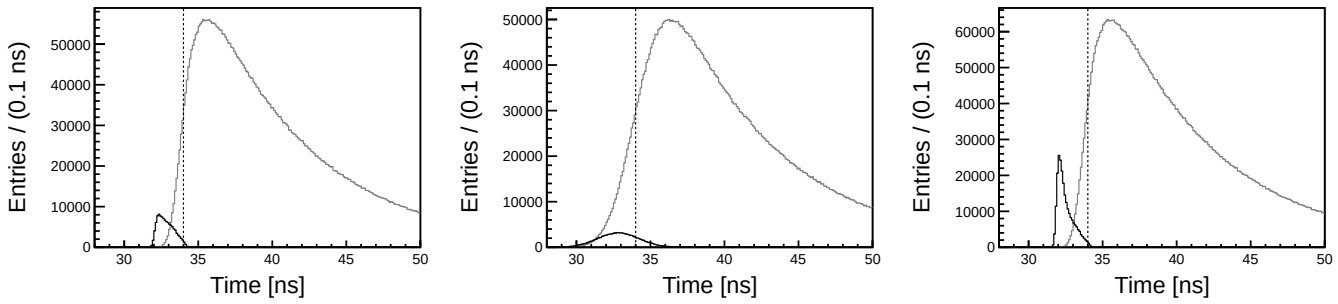

(a) Default simulation. (b) Increased TTS (1.28 ns). (c) Red-sensitive photocathode.

FIG. 2: PE times after TTS application for the simulation of 1000 electrons (5 MeV) with different settings. PEs from Cerenkov light (black) and scintillation light (grey) are compared. The dashed vertical line illustrates a time cut at 34 ns. (a) Default simulation: bialkali photocathode and TTS = 0.1 ns (σ). After the 34.0 ns time cut we get 171 PEs from scintillation and 108 PEs from Cerenkov light. (b) Default simulation settings except for TTS = 1.28 ns (KamLAND 17 in. PMTs). After the 34.0 ns time cut we get 349 PEs from scintillation and 88 PEs from Cerenkov light. (c) Default simulation settings except for a GaAsP photocathode. After the 34.0 ns time cut we get 226 PEs from scintillation and 229 PEs from Cerenkov light.

of scintillation rise time which is the reason why there is a lack of accurate numbers. We assume a rise time of 1.0 ns, more detailed studies are needed in the future. The two time constants used to describe the falling edge of the scintillator emission time distribution (quoted above) are values specific to the KamLAND scintillator. Third, chromatic dispersion turns out to be an important effect in a 6.5 m diameter detector at the level of precision needed for direction reconstruction. Due to the wavelength-dependence of the refractive index the speed of light in the scintillator (see Equation (2)) increases with increasing photon wavelengths for normal dispersion. In order to study the size of this effect, we extracted results from a simplified simulation of 5 MeV electrons at the center of the sphere where we used instantaneous scintillation and applied QE but no TTS. The true hit time distributions of photoelectrons were analyzed for scintillation light and Cerenkov light separately. Photoelectrons coming from Cerenkov light are on average created about 0.5 ns earlier than PEs from scintillation light. The RMS values for both the Cerenkov and scintillation light true PE time distributions are both about 0.5 ns. Note that these numbers include the effect of the finite electron travel time.

On the detector side, the time information of single photoelectrons is affected by the TTS of the photodetectors, a number which can be different by orders of magnitude depending on the detector type. The default TTS of 0.1 ns (σ) is a value which can be achieved with the large area picosecond photodetectors (LAPPDs)[25, 26] and possibly hybrid photodetectors (HPDs)[27]. In fact, even significantly lower TTS numbers are realistic with the LAPPD. Finally, the accuracy of the vertex reconstruction is reflected in broadening and distortions of the time spectrum (after time-of-flight correction has been applied). Another effect which is to be addressed in future work is the granularity of the photodetectors which adds to the uncertainty in the light path and thus the time-of-flight correction.

In Sections IV to VI, we comparatively study the photoelectron timing for different detector configurations. We follow the idea to increase discrimination between Cerenkov and scintillation light by accurate detector timing. The main relevant quantities provided by the Geant4 simulation are the photoelectron hit positions and the detection times after TTS has been applied. In section VII these quantities are used for event reconstruction.

IV. DETECTOR TIMING

First we discuss results for the default simulation settings which are described in the previous section. Figure 2 (a) shows the TTS-smeared photoelectron detection times for 1000 simulated electrons with 5 MeV energy in the center of the detector with initial momentum direction coinciding with the x-axis. The photoelectrons induced by Cerenkov light arrive earlier, as expected due to the instantaneous emission and the higher average photon speed (higher wavelengths) compared to scintillation after QE weighting. There is however significant overlap with the PE time distribution coming from scintillation light. In order to compare simulations with different parameters to each other a fixed time cut $t \leq 34.0$ ns (or 33.0 ns) is applied using the truth information of the electron starting time instead of an event-by-event time reconstruction (see Section VII for reconstruction results). For the default simulation case, the number of PEs per event coming from Cerenkov light after the 34.0 ns time cut (108) is 98 % of the total number of PEs from Cerenkov light (110). For scintillation the number of PEs after the time cut (171) is only 3.2 % of the total scintillation-induced PEs (5445). This indicates the effectiveness of a time cut to separate Cerenkov light from scintillation light. An important figure of merit when comparing different simulation settings is the ratio of Cerenkov/scintillation induced PE after the 34.0 ns time cut since a higher ratio means more directional information per PE. The ratio is 0.63 for the default settings. Note that this

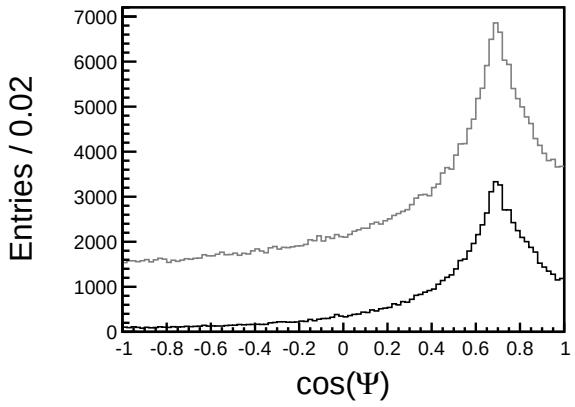

FIG. 3: Angular distribution of photoelectron hits relative to the original electron direction along the x-axis: $\cos(\Psi) = x_{hit}/\vec{r}_{hit}$. 1000 electron events with 5 MeV at the center are summed. Default simulation settings are used and both Cerenkov and scintillation light are included. A 33.0 ns time cut (black) is compared with a 34.0 ns time cut (grey).

ratio depends on the time cut, which will be optimized in future work together with the absolute number of PEs per event passing the cut.

Figure 3 displays the PE hit pattern after cutting on time. Although this time cut is a simplification of actual time reconstruction effects, we can use it to indicate the spatial distribution of hits after timing information has been used to separate Cerenkov and scintillation light. The Cerenkov ring structure can be clearly seen (peak at about 46°) which demonstrates that the directional signal conveyed by the Cerenkov photons is not erased by scattering of the initial 5 MeV electrons.

If the 17 inch KamLAND PMTs [21, 28] (TTS = 1.28 ns) are used in the simulation, the broadening of the time distributions leads to a strongly decreased ratio of Cerenkov over scintillation light (0.25) after the 34 ns time cut (see FIG. 2 (b)). This shows that low photodetector TTS is critical for directionality reconstruction and motivates the use of novel detector types.

V. DETECTOR WAVELENGTH RESPONSE

Complementary to lowering the photodetector TTS, optimization of the wavelength-dependent QE is promising. Since Cerenkov photons which passed 6.5 m of scintillator have higher average wavelengths than scintillation photons, a photodetector which is more sensitive at high wavelengths increases not only the absolute number of PEs but also the ratio between Cerenkov- and scintillation-induced PEs. Therefore, a simulation has been run with the QE of an extended red-sensitive GaAsP photocathode (Hamamatsu R3809U-63 QE data was used).

Figure 2 (c) shows the results for the modified simulation with high QE in the red spectral region. The higher absolute number of PE coming from Cerenkov light (factor of ≈ 2) and the increased Cerenkov/scintillation ratio (1.6) after the time cut would significantly enhance the directionality reconstruction capabilities given that high coverage can be achieved with red-sensitive photocathodes.

VI. SCINTILLATOR EMISSION SPECTRUM

An alternative route towards increasing the separation in time between Cerenkov and scintillation photon hits is the tuning of the scintillator emission spectrum. Recently, the use of quantum dots (QDs) in liquid scintillators has been studied as a possibility to improve future large scale neutrino experiments [29]. One major motivation for quantum-dot-doped scintillator is control of the emission spectra by tuning the size or composition of the quantum dots. The emission spectrum of commercial alloyed core/shell CdS_xSe_{1-x}/ZnS quantum dots was measured. This spectrum shows a symmetric peak centered around 461 nm with FWHM = 29 nm.

In order to isolate the effect of a different emission spectrum, the other simulation settings, including the KamLAND absorption spectrum are kept unchanged. Compared to the default case shown in FIG. 2 (a) the separation is worse (as expected) because the scintillation light wavelengths are higher than in the KamLAND emission spectrum. However, advances in the production of commercial quantum dot samples could yield quantum dots which have similar, single peak emission shapes at lower wavelengths. This case has been simulated using the same spectral shape of the measured core-shell quantum dot emission but shifted to lower wavelengths such that the emission peak is centered at 384 nm. This peak emission value has been measured for other types of QDs, however with a much more pronounced tail [29]. The resulting PE time distribution shows improved separation of Cerenkov and scintillation light compared to the default simulation. After the 34.0 ns cut on the TTS-smeared PE time we obtain a higher Cerenkov/scintillation ratio of 0.86 (107 PE from Cerenkov light and 124 PE from scintillation). The number of Cerenkov-induced PE after the time cut is unchanged while the number of PEs coming from scintillation light is decreased due to the higher average photon travel times.

VII. RECONSTRUCTION

WCSimAnalysis is a Water Cherenkov reconstruction package developed by Andrew Blake for the Long Baseline Neutrino Experiment (LBNE collaboration) [30]. It provides a framework for generic event cleaning, track reconstruction, and particle identification, and it comes equipped with variety of pre-built algorithms. A collaboration between Iowa State, the University of Chicago, and Argonne National Laboratory has continued adding to the code, developing new track-fitting techniques for Water Cherenkov detectors based on advanced photosensors with sub-cm imaging capabilities and timing resolutions below 100 picoseconds [31, 32]. In this paper, we use only the simple, low-level reconstruction

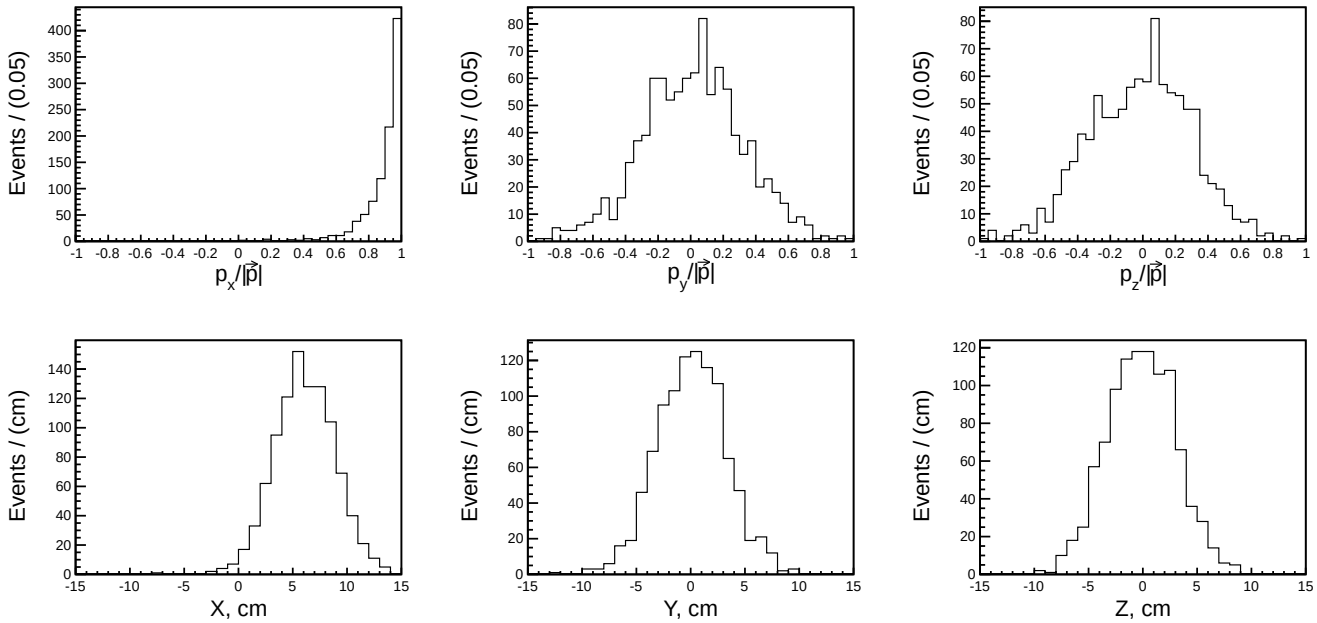

FIG. 4: (Top) Reconstructed direction, $(\frac{p_x}{|\vec{p}|}, \frac{p_y}{|\vec{p}|}, \frac{p_z}{|\vec{p}|})$, for the simulation of 1000 electrons (5MeV). In the simulation the electrons are produced along the X-axis, $\frac{\vec{p}}{|\vec{p}|}$ = (1,0,0), and originate from the center of the detector, $\vec{r}$ = (0,0,0). Detector diameter, R = 6.5 m. Only photons with arrival time of $T < 34$ ns are used in the reconstruction. The quantum efficiency of the bialkali photocathode is taken into account. (Bottom) Reconstructed vertex position, (x, y, z), for the simulation of 1000 electrons (5 MeV). In the simulation the electrons are produced along the x-axis, $\frac{\vec{p}}{|\vec{p}|}$ = (1,0,0), and originate from the center of the detector, $\vec{r}$ = (0,0,0). Detector diameter, R = 6.5 m. Only photons with arrival time of $T < 34$ ns are used in the reconstruction. The quantum efficiency of the bialkali photocathode is taken into account.

tools native to the package, though in future works we hope to implement more sophisticated algorithms.

The results presented in this paper rely on a simple vertex reconstruction algorithm, commonly known as a "point fit" [33]. It assumes that all of the scintillation and Cherenkov light is emitted from a single point in space-time (x_0, y_0, z_0, t_0). In actuality, the light is emitted along an extended, multi-scattered electron track. However, at the energies discussed in this paper, the extent of this track is small (a few cm) compared to the scale of the detector (R=6.5 meters) and thus typical photon transit distances.

The first step of the reconstruction process relies on exact numerical calculations of vertex candidates from quadruplets of hits. Given a single point source, we need four constraints to solve for the four unknowns of the vertex [34]. This approach would provide an exact solution in the case of four prompt, unscattered photons originating from a common point. However, many of these randomly chosen quadruplets will produce anomalous solutions due to real world effects such as delayed emission and deviations from the point-like geometry. Nonetheless, we found that any chosen subset of 400 quadruplets was a sufficiently large ensemble to assure that some solutions will be close to the true vertex.

Once a small set of vertex candidates have been solved for, we test the goodness of each candidate and select the one that best fits the full ensemble of photon hits. The goodness of fit is determined based on the distribution of an observable known as the "point time residual" [33]. The point time residual is calculated by taking the difference between the measured time of a photon hit, and the predicted time of the hit, given its distance from the vertex hypothesis, the speed of light in the scintillator, and the hypothesized t_0 of the event. The width of the time residual distribution over all hits is minimized when the hypothesized vertex is near the true vertex. Based on this figure of merit, we select the vertex with the narrowest time residual distribution from among the 400 candidates. This best candidate is used as the seed value for a MINUIT-based optimization [35], where the vertex is allowed to vary over a continuum of locations until the global optimum is found.

The direction of the electron track is determined by taking the centroid of all vectors pointing from the fitted vertex to the hits on the detector. Since the Cherenkov light his highly directional, and since our timing cut enhances the purity of the Cherenkov light in the sample, this calculation provides a good measure of the track direction. Future work will focus on more sophisticated algorithms, taking better advantage of the highly constrained Cherenkov geometry. For the purpose of this paper, the current method provides a very good proof-of-principle.

For the purpose of testing the reconstruction algorithm described above we use 1000 simulated electrons with the energy of 5 MeV. The electrons are similated at the center of the detector, $\vec{r}$ = (0,0,0), along the x-axis, $\frac{\vec{p}}{|\vec{p}|}$ = (1,0,0).

Figure 4 show vertex reconstruction. The vertex is rea-

sonably well reconstructed around center of the detector, $\vec{r}$ = (0,0,0). The RMS of the distributions for all three reconstructed coordinates are smaller than 3.5 cm. The shift along x-axis is attributed to the fact that electron is moving towards that direction and has a finite track length while the reconstruction algorithm treats all photons as they were emitted from the same point.

The reconstruction of the direction is shown in Fig. 4. For majority of the events we are able to reconsruct the direction along x-axis.

VIII. CONCLUSION

The ability to reconstruct direction in kiloton-scale scintillating detectors would be a major technological advance. It would find immediate application in neutrino experiments especially those searching for $0\nu\beta\beta$. More generally, this technique could be applied wherever scintillation-based detectors are used. A Geant4 simulation of a simple spherical detector corresponding to a kiloton of scintillator shows that timing on the order of 0.1 ns is required to separate the directional Cerenkov light from the more abundant scintillation light. This separation can be improved using photodetectors with more red sensitivity and liquid scintillators with a more narrow emission spectrum shifted to shorter wavelengths. Furthermore, simple reconstruction algorithms adapted from those for water Cerenkov detectors are able to reliable reconstruct the position and direction of 5 MeV electrons. More detailed simulation and advanced reconstruction algorithms will need to be developed to move to lower energies and more complicated event topography, like those in $0\nu\beta\beta$, but the technique already appears very promising.

IX. ACKNOWLEDGEMENTS

We would like to thank and acknowledge Andrew Blake at University of Cambridge for his work authoring the WCSimAnalysis code used to perform the reconstructions shown in this paper. Special thanks to the neutrino reconstruction group at Iowa State, particularly Mayly Sanchez, Ioana Anghel, and Tian Xin for their continued work in developing the WCSimAnalaysis algorithms and for their insights and expertise regarding issues related to Cherenkov reconstruction with fast-timing. Thanks also to Micheal Smy for his development of the quadruplet-based, vertex-finding method. L. Winslow would like to thank J.M. Conrad for useful discussion on the topic. L. Winslow would also like to thank K. Arisaka for discussions on the possible reach of traditional PMTs and the characteristics of HPDs. A. Elagin, H.J. Frisch and M. Wetstein are supported by DOE XXXX. C. Aberle and L. Winslow are supported by funds from University of California Los Angeles.

[1] KamLAND Collaboration, A. Gando *et al.*, (2013), 1303.4667.
[2] G. Bellini *et al.*, Phys.Rev.Lett. **107**, 141302 (2011), 1104.1816.
[3] Daya Bay Collaboration, F. An *et al.*, Chin. Phys. **C37**, 011001 (2013), 1210.6327.
[4] Double Chooz Collaboration, Y. Abe *et al.*, Phys.Rev. **D86**, 052008 (2012), 1207.6632.
[5] Double Chooz Collaboration, Y. Abe *et al.*, Phys.Lett. **B723**, 66 (2013), 1301.2948.
[6] RENO, J. K. Ahn *et al.*, Phys. Rev. Lett. **108**, 191802 (2012).
[7] Y.-F. Li, J. Cao, Y. Wang, and L. Zhan, (2013), 1303.6733.
[8] RENO-50 - International Workshop on toward Neutrino Mass Hierarchy, 2009.
[9] J. Conrad *et al.*, Precision $\bar{\nu}_e$-electron Scattering Measurements with IsoDAR to Search for New Physics, In preparation, for submission to PRD., 2013.
[10] IsoDAR, A. Bungau *et al.*, (2012), 1205.4419.
[11] K. Heeger, B. Littlejohn, and H. Mumm, (2013), 1307.2859.
[12] A. Porta *et al.*, Nuclear Science, IEEE Transactions on **57**, 2732 (2010).
[13] N. Bowden *et al.*, Nuclear Instruments and Methods in Physics Research Section A: Accelerators, Spectrometers, Detectors and Associated Equipment **572**, 985 (2007).
[14] KamLAND-Zen Collaboration, A. Gando *et al.*, Phys.Rev.Lett. **110**, 062502 (2013), 1211.3863.
[15] J.B. Birks, *The Theory and Practice of Scintillation Counting* (Pergamon Press, 1964).
[16] L. Winslow and R. Simpson, Journal of Instrumentation **7**, P07010 (2012).
[17] A. M. Steinberg, P. G. Kwiat, and R. Y. Chiao, Phys. Rev. Lett. **68**, 2421 (1992).
[18] GEANT4, S. Agostinelli *et al.*, Nucl.Instrum.Meth. **A506**, 250 (2003).
[19] J. Allison *et al.*, Nuclear Science, IEEE Transactions on **53**, 270 (2006).
[20] KamLAND, K. Eguchi *et al.*, Phys.Rev.Lett. **90**, 021802 (2003), hep-ex/0212021.
[21] O. Tajima, Development of liquid scintillator for a large size neutrino detector, Master's thesis, Tohoku University, 2000.
[22] O. Perevozchikov, *Search for electron antineutrinos from the sun with KamLAND detector*, PhD thesis, University of Tennessee, 2009.
[23] O. Tajima, *Measurement of Electron Anti-Neutrino Oscillation Parameters with a Large Volume Liquid Scintillator Detector, KamLAND*, PhD thesis, Tohoku University, 2003.
[24] C. Grant, *A Monte Carlo Approach to ^{7}Be Solar Neutrino Analysis with KamLAND*, PhD thesis, University of Alabama, 2012.
[25] J. Anderson *et al.*, The Development of Large-Area Fast Photodetectors, 2009.
[26] LAPPD Collaboration, Technical Design Report for the frugal MCP, 2010.
[27] Y. Kawai, *Development of a Hybrid Photon-Detector Module for Next Generation Water-Cherenkov Detectors Yoshihiko*, PhD thesis, The Graduate University for Advenced Studies (SOKENDAI), 2007.
[28] H. Kume *et al.*, Nucl.Instrum.Meth. **205**, 443 (1983).
[29] C. Aberle, J.J. Li, S. Weiss, L. Winslow, arXiv:1307.4742 [physics.ins-det].
[30] A. Blake, *WCSimAnalaysis Reconstruction Package*, Cavendish Laboratory, University of Cambridge, UK.

[31] M. Sanchez *et al.*, Fast-timing neutrino reconstruction group.
[32] The Large Area Picosecond Photodetector Collaboration.
[33] M. Ishitsuka, *L/E Analysis of the Atmospheric Neutrino Data From Super-Kamiokande*, PhD thesis, University of Tokyo, 2004.
[34] M. Smy, *Bonsai: Low Energy Vertex Reconstruction for DUSEL LBNE*, a talk presented to the LBNE collaboration (2010).
[35] F. James and M. Roos, CERN Program Library Long Writeup **D506** (1992).